Biochemical characterisation and novel classification of monofunctional *S*-adenosylmethionine decarboxylase of *Plasmodium falciparum*

Marni Williams[a], Janina Sprenger[b,c], Esmaré Human[a], Salam Al-Karadaghi[c], Lo Persson[b], Abraham I. Louw[a], Lyn-Marie Birkholtz[a,*]

[a] *Department of Biochemistry, University of Pretoria, Private Bag X20, Hatfield 0028, South Africa*

[b] *Department of Experimental Medical Science, Lund University, S-221 84 Lund, Sweden*

[c] *Department of Biochemistry and Structural Biology, Centre for Molecular Protein Science, Lund University, S-221 00 Lund, Sweden*

[*] Corresponding author at:

Department of Biochemistry, University of Pretoria, Private Bag X20, Hatfield 0028, South Africa.

Tel.: +27 12 420 2479; fax: +27 12 362 5302.

E-mail address: lbirkholtz@up.ac.za (L. Birkholtz).

Abstract

Plasmodium falciparum like other organisms is dependent on polyamines for proliferation. Polyamine biosynthesis in these parasites is regulated by a unique bifunctional *S*-adenosylmethionine decarboxylase/ornithine decarboxylase (PfAdoMetDC/ODC). Only limited biochemical and structural information is available on the bifunctional enzyme due to the low levels and impurity of an instable recombinantly expressed protein from the native gene. Here we describe the high level expression of stable monofunctional PfAdoMetDC from a codon-harmonised construct, which permitted its biochemical characterisation indicating similar catalytic properties to AdoMetDCs of orthologous parasites. In the absence of structural data, far-UV CD showed that at least on secondary structure level, PfAdoMetDC corresponds well to that of the human protein. The kinetic properties of the monofunctional enzyme were also found to be different from that of PfAdoMetDC/ODC as mainly evidenced by an increased K_m. We deduced that complex formation of PfAdoMetDC and PfODC could enable coordinated modulation of the decarboxylase activities since there is a convergence of their k_{cat} and lowering of their K_m. Such coordination results in the aligned production of decarboxylated AdoMet and putrescine for the subsequent synthesis of spermidine. Furthermore, based on the results obtained in this study we propose a new AdoMetDC subclass for plasmodial AdoMetDCs.

Keywords: codon-harmonize, *S*-adenosylmethionine decarboxylase, malaria, oligomerization, polyamines

Abbreviations: AdoMet, *S*-adenosyl-L-methionine; AdoMetDC, *S*-adenosylmethionine decarboxylase; CGP48664, 4-amidinoindan-1-one-2'-amidinohydrazone; dcAdoMet, decarboxylated *S*-adenosyl-L-methionine; DLS, dynamic light scattering; far-UV CD, far ultraviolet circular dichroism; *harmA/wtO*, harmonised *S*-adenosylmethionine decarboxylase/ wild-type ornithine decarboxylase; Hsp70, *E. coli* heat shock protein 70; MDL73811, 5'-([(Z)-4-amino-2-

butenyl]methylamino)-5'-deoxyadenosine); ODC, ornithine decarboxylase; SEC, size-exclusion chromatography.

1. Introduction

The polyamines putrescine, spermidine and spermine are aliphatic, low-molecular weight nitrogenous bases that can form electrostatic interactions with anionic molecules such as nucleic acids, proteins and lipids [1]. They are involved in many growth processes including cell differentiation, proliferation [2, 3] and apoptosis [4, 5]. Polyamine concentrations are strictly regulated on transcriptional, translational and post-translational levels as well as by uptake and efflux processes [1]. Erythrocytes infected by *Plasmodium falciparum* (the causative agent of fatal malaria) contain high levels of polyamines during stages of rapid growth [6, 7]. In *Plasmodium* spp, polyamine biosynthesis is uniquely characterised by the bifunctional arrangement of the rate-limiting decarboxylases, *S*-adenosylmethionine decarboxylase (PfAdoMetDC) and ornithine decarboxylase (PfODC) in a single protein, PfAdoMetDC/ODC [8]. The PfAdoMetDC and PfODC domains within PfAdoMetDC/ODC catalyze the synthesis of decarboxylated *S*-adenosyl-L-methionine (dcAdoMet) from AdoMet and putrescine from L-ornithine, respectively. dcAdoMet then provides an aminopropyl moiety for the synthesis of spermidine from putrescine in a reaction catalysed by spermidine synthase.

The *PfAdometdc/Odc* gene encodes a 1419 residue polypeptide that is maintained as a single, bifunctional protein with a hinge region (275 residues) connecting the 530-residue PfAdoMetDC domain (N-terminus) to the 614-residue PfODC domain (C-terminus) [8]. Both of these decarboxylase activities function independently of each other within the bifunctional complex [9], although it was shown that inter- and intradomain interactions modulate both activities [10]. In contrast to their single-enzyme orthologues in other organisms, the PfODC activity in the bifunctional enzyme is strongly feedback-inhibited by putrescine, whereas PfAdoMetDC activity is not stimulated by putrescine [9, 11]. In the absence of known regulatory mechanisms that control polyamine levels in other organisms, the presence of a single PfAdoMetDC/ODC polypeptide has been suggested to allow regulation of polyamine pools in plasmodia [9].

AdoMetDC from various organisms are classified into five distinct subclasses based on their oligomeric structure, mechanism of autocatalytic processing and activation factors [12, 13]. Of

these, only the crystal structures of human (*Homo sapiens*), plant (*Solanum tuberosum*) and prokaryotic (*Thermotoga maritima*) AdoMetDCs have been solved [14-16]. The quaternary structure of the human monomeric protein revealed a novel four-layer αββα-sandwich domain, which exists as an $(\alpha\beta)_2$ dimer where the α- and β-subunits are formed by an autocatalytic processing event (non-hydrolytic serinolysis). Processing results in the simultaneous formation of the active site pyruvoyl cofactor at Ser68 [16]. In the case of plasmodial AdoMetDC, homology models predicted a similar α/β-fold to that of the human protein for the monofunctional PfAdoMetDC [11] but other properties e.g. oligomeric status or catalytic mechanism were not elucidated.

In this study, soluble and active monofunctional PfAdoMetDC was expressed from a codon-harmonised construct in sufficient purity and quantity for its biochemical and biophysical characterisation. We show that the monofunctional enzyme is able to dimerise but this is not essential for activity of the enzyme and that monofunctional PfAdoMetDC has similar kinetic properties compared to homodimeric kinetoplastid AdoMetDCs. These results offer a novel insight into a likely mechanism where the enzyme activities of PfAdoMetDC and PfODC are concurrently modulated in the bifunctional protein to align the rate of delivery of the two substrates required for downstream biosynthesis of spermidine. In addition, a comparison to the structurally characterised AdoMetDCs from other organisms, illustrates differences in the oligomeric status, mechanism of regulation and autocatalytic processing of PfAdoMetDC, which necessitates the introduction of a novel subclass for plasmodial AdoMetDC, namely 2b-III.

2. Materials and methods

2.1 Cloning of codon-harmonised monofunctional PfAdometdc and bifunctional PfAdometdc/Odc

Codon harmonisation was used for production of heterologously expressed monofunctional PfAdoMetDC in *E. coli*. The codon harmonisation algorithm is implemented in a PHP-script driven

web interface and is available at http://www.sami.org.za/equalize. Synonymous codons were chosen to ensure that the positional codon frequency of low/intermediate and high usage codons are similar to the frequency used by that of the *E. coli* host [17]. Codon-harmonised nucleotides 1-1461 (GeneArt, Regensburg, Germany) encoding the core of PfAdoMetDC (487 residues) [11] was used to replace the corresponding wild-type (wt) sequence within *PfAdometdc/Odc* (*wtA/wtO*, GENBANK ID: Q8IJ77) in pASK-IBA3 [8] to create a full-length, partially harmonised *PfAdometdc*/*Odc* construct (*harmA/wtO)*. From this construct the first 1461 harmonised nucleotides and an additional 255 wild-type nucleotides were amplified with sense (5'-ATGGTAGGTCTCAAATGAATGGCATTTTCGAAGGCATTGAAA-3') and antisense (5'-ATGGTAGGTCTCAGCGCTCAAAGTTTCTTTTTCTACACATTTAAC-3') primers. The resultant fragment was subcloned into the *Bsa*I site of pASK-IBA3 (C-terminal Strep-tag) to create a construct encoding monofunctional PfAdoMetDC (572 residues). Protein expression from this harmonised construct was compared to the expression of a protein from the wild-type gene (construct provided by Dr. C. Wrenger [9]), which encodes half of the hinge region (wtPfAdoMetDC-hinge, 660 residues) with an N-terminal Strep-tag. In addition, expression of the full-length PfAdoMetDC/ODC proteins from the pASK-IBA3 constructs containing *harmA/wtO* and *wtA/wtO* [8] were also compared. All sequences were verified by Sanger dideoxy nucleotide sequencing.

2.2 Protein expression and purification

The monofunctional PfAdoMetDC and wtPfAdoMetDC-hinge [9] as well as the bifunctional PfAdoMetDC/ODC (encoded by *harmA/wtO* and *wtA/wtO*) proteins were expressed in BL21 Star™ cells (Invitrogen). Protein purification using Strep-*Tactin* affinity matrix (IBA) was performed as described previously [10]. Protein bands separated by SDS-PAGE and visualised with Colloidal Coomassie or silver staining were identified with LC-MS/MS [18]. The monofunctional proteins

separated with SDS-PAGE were also identified with Western immunodetection using monoclonal Strep-tag II mouse antiserum conjugated to horseradish peroxidase (Acris antibodies) [10].

The affinity-purified PfAdoMetDC protein sample was further separated with size-exclusion chromatography (SEC) using an Äkta Explorer System (Amersham Pharmacia Biotech). A Superdex®-S200 10/300 GL SE column (Tricorn, GE Healthcare) was calibrated with the Gel Filtration Standard kit (BioRad) and equilibrated with wash buffer (100 mM Tris/HCl pH 8.0, 150 mM NaCl, 1 mM EDTA). Protein samples (500 µL) were loaded and fractions corresponding to the $(\alpha\beta)_2$ dimeric (estimated size of 140 kDa) and (αβ) monomeric (~70 kDa) PfAdoMetDC were collected, pooled and subsequently concentrated with Amicon Ultra centrifugal filter devices (MWCO 3000, Millipore). Enzyme concentration was determined by UV absorbance measurements at 280 nm with an extinction coefficient of 69110 M^{-1} cm^{-1}.

2.3 PfAdoMetDC activity assays

The PfAdoMetDC and wtPfAdoMetDC-hinge proteins were assayed for enzyme activity directly after purification and after two weeks of storage at 4 and -20 °C. The assays contained 5 µg enzyme, 100 µM *S*-adenosyl-L-methionine chloride (Sigma-Aldrich) and 50 nCi *S*-[carboxy-^{14}C]adenosyl-L-methionine (55 mCi/mmol, Amersham Biosciences) in a total volume of 250 µL assay buffer (50 mM KH_2PO_4 pH 7.5, 1 mM EDTA, 1 mM DTT) and were performed as previously described [8]. Experiments were performed in duplicate for three individual experiments and specific enzyme activities were expressed as the amount of CO_2 produced in nmol/min/mg or nmol/min per nmol protein when constructs with different sizes were compared. Statistical analysis was performed using the paired Students t-test with $P<0.05$ indicating statistical significance.

2.4 Oligomeric status analyses with SEC

The oligomeric status of affinity-purified PfAdoMetDC at concentrations of 1 mg/mL and 4 mg/mL was analysed with SEC under non-reducing conditions. Reducing SEC was also performed

by equilibrating the SEC column with wash buffer containing 10 mM DTT. Monomeric and dimeric protein fractions collected from SEC were analysed in terms of their elution volumes (V_e) relative to the void volume (V_o) of the column (V_e/V_o). The SEC-purified fractions were also visualised with reducing (10 mM DTT added to the sample buffer immediately prior to gel loading and electrophoresis) and non-reducing SDS-PAGE. Peptide mass fingerprinting with MALDI-MS was performed on the bands corresponding to the monomeric and dimeric proteins. Protein sample extraction, dehydration and preparation for MALDI-MS as well as sample derivatisation with 55 mM iodoacetamide to identify Cystines possibly involved in disulphide-bond formation, was performed as described [19, 20]. The reduced protein sample for MS was obtained by pre-treatment with 10 mM DTT for 30 min at 37 °C followed by alkylation and trypsin digestion.

To estimate the order of magnitude of the dissociation constant (K_D) of the PfAdoMetDC dimer for comparison to other AdoMetDCs, the relative peak heights of the monomeric and dimeric proteins in the non-reducing SEC elution profiles were assumed to approximately represent the relative proportions of monomer and dimer in the samples. Since the total amount of protein loaded was known, the concentrations of the monomeric and dimeric proteins could be determined based on their relative proportions. The formulae that were applied are given in Table 1.

2.5 Site-directed mutagenesis

Based on the MALDI-MS results obtained above, the role of Cys505 in dimer stabilisation via covalent disulphide bond formation was studied by replacing it with a Ser residue to create the C505S mutant. Site-directed mutagenesis was performed by using harmonised *PfAdometdc* cloned into the pASK-IBA3 vector as template. Ex Taq™ DNA Polymerase (Takara Bio Inc.) was used to amplify the entire template in the presence of 6 fmol template and 10 pmol of each of the sense (5'-GGTAAAAGTTCCGTTTATTATCAAG-3') and antisense (5'-CTTGATAATAAACGGAACTTTTACC-3') primers (mutations are underlined). Temperature cycling was performed as follows: 95 °C for 3 min followed by 25 cycles of 96 °C for 30 s, 56 °C

for 30 s, 68 °C for 5 min with a final extension step at 68 °C for 10 min. Post-PCR manipulation was performed as described previously [21]. The expressed protein was analysed with an enzyme assay, SDS-PAGE and SEC as described above.

2.6 Dynamic Light Scattering

The hydrodynamic radii of the PfAdoMetDC and C505S mutant proteins were determined by dynamic light scattering (DLS) as an indication of their oligomeric status. Fractions of the proteins collected after SEC were pooled and concentrated to 2.5-5 mg/mL. The PfAdoMetDC proteins were also analysed after treatment with 10 mM DTT prior to the DLS measurement. Immediately prior to measurements, the samples were centrifuged for 10 min at 10,000 x *g* to remove any aggregates. DLS was measured with the default settings of the Nanoziser Nano S instrument (Malvern Instruments). A 3 mm precision cell cuvette (Hellma) was used in which the protein samples with volumes of 15 µL were pre-equilibrated for 5 min at 20 °C. The Zetasizer Nano software v6.01 with default settings was used to determine the particle size distribution as given by the volume intensity plot.

2.7 Far-UV CD spectroscopy

The PfAdoMetDC and C505S mutant proteins in wash buffer collected from SEC were dialyzed against a phosphate buffer (10 mM KH_2PO_4 pH 7.7, 50 mM NaF) prior to far-ultraviolet (UV) circular dichroism (CD) analysis [22]. Results from DLS confirmed that this buffer did not cause protein aggregation or affected the oligomeric state of the proteins.

The far-UV spectra of the PfAdoMetDC and C505S mutant proteins (0.5 mg/mL) were determined with the JASCO J815 CD instrument. Measurements were conducted in 1 mm quartz cell at a wavelength range of 190 to 250 nm at 20 °C using a wavelength interval of 0.5 nm, a bandwidth of 1 nm and a scanning speed of 20 nm/min. Two readings were accumulated per sample, buffer spectra were subtracted and the data points were averaged. The molar ellipticity

($[\theta]_M$) of each data point is given in units deg cm^2 $dmol^{-1}$ as calculated in the study by Bale *et al*. [23]. The secondary structure content was calculated with the use of CDtool v1.4 [24].

2.8 PfAdoMetDC enzyme and inhibition kinetics

The substrate affinity constant as well as V_{max} of PfAdoMetDC was determined using Michaelis-Menten kinetics. A substrate dilution series ranging from 12.5 to 800 µM was used for the Michaelis-Menten curve and the linear Hanes-Woolf plot was used to determine the K_m and V_{max} values [25]. Three independent experiments were performed in duplicate using the enzyme assay described above and the results were analysed with GraphPad Prism v5.0 (GraphPad Software, Inc.).

The rate of enzyme inactivation by the irreversible inhibitor MDL73811 (5'-([(Z)-4-amino-2-butenyl]methylamino)-5'-deoxyadenosine) [26] was followed by measurement of residual activity after fixed time intervals (0, 2, 4 and 6 min) of exposure to the inhibitor. The PfAdoMetDC enzyme (1 µg) was mixed with 0.1, 0.2 and 0.5 µM MDL73811 in assay buffer and incubated for 0-6 min at 37 °C for these assays. A secondary plot of the reciprocal of the k_{app} value (-1/primary slope) for each inhibitor concentration against the reciprocal of the concentration used, resulted in a straight line from which the k_{inact} and K_i values could be determined by the intercept and slope, respectively [27].

The inhibition of PfAdoMetDC with the substrate analogue CGP48664 (4-amidinoindan-1-one-2'-amidinohydrazone) [28] was assayed using different substrate (100, 200, 400 and 800 µM) and inhibitor (0, 2.5, 5 and 10 µM) concentrations for 30 min at 37 °C. The results were plotted on a typical Michaelis-Menten plot to obtain several hyperbolic curves for each inhibitor concentration at increasing substrate concentrations.

3. Results

3.1 Soluble expression of monofunctional PfAdoMetDC

In this study, the heterologous expression of codon-harmonised *PfAdometdc* in BL21 Star™ cells was compared to that of the protein expressed from *wtPfAdometdc-hinge* [9]. Denaturing SDS-PAGE followed by LC-MS/MS identification of the specific bands showed that while the ~9 kDa β-subunit was not resolved, the α-subunit of the wtPfAdoMetDC-hinge protein at ~70 kDa (Fig. 1A, lane 1) co-purified with an approximately equal amount of *E. coli* heat shock protein 70 (Hsp70) (Fig. 1A, lane 1). However, expression from the harmonised *PfAdometdc* gene resulted in an almost 10-fold improvement in protein expression yield of particularly the α-subunit (~60 kDa) of the monofunctional PfAdoMetDC protein (Fig. 1A, lane 2). This was confirmed by Western immunodetection using an anti-Strep-tag antibody (Fig. 1B, lane 2). The C-terminal-Strep tag remained attached to the larger ~60 kDa α-subunit following autocatalytic processing at residue Ser73. The ~69 kDa protomer of PfAdoMetDC, which has not undergone autocatalytic processing, was also detected. The wtPfAdoMetDC-hinge protein was not detected by Western blotting due to the separation of the ~70 kDa α- and the ~9 kDa β-subunits, which carries the N-terminal Strep-tag (Fig. 1B, lane 1).

Monofunctional PfAdoMetDC is enzymatically active with a specific activity of 140±8 nmol/min per nmol protein compared to wtPfAdoMetDC-hinge with an activity of 88±4 nmol/min/nmol of which approximately half of the protein sample contains Hsp70 (Fig. 1A, lane 1). Furthermore, PfAdoMetDC appeared to be a more stable protein than wtPfAdoMetDC-hinge since activity was maintained after storage for two weeks at 4 and -20 °C. In contrast, the wtPfAdoMetDC-hinge activity was significantly reduced by 16% and 55% (n=2, $P<0.05$) at 4 and -20 °C, respectively. In addition, expression of the complete bifunctional PfAdoMetDC/ODC from the *harmA*/*wtO* gene resulted in an PfAdoMetDC activity of 22±1.2 nmol/min/mg compared to only 6.8±0.1 nmol/min/mg when the bifunctional protein was expressed from the *wtA*/*wtO* gene construct (n=4).

Based on the protein expression and activity results, all subsequent experiments were performed on the pure and stable monofunctional PfAdoMetDC protein expressed from the harmonised gene.

3.2 Monomer-dimer equilibration studies of PfAdoMetDC

Strep-*Tactin* affinity chromatography-purified PfAdoMetDC was further analysed by SEC to determine its oligomeric status. Concentration-dependent monomer-dimer equilibrium is evident since at 1 mg/mL both monomeric (V_e/V_o of 1.77, ~85 kDa) and dimeric (V_e/V_o of 1.59, ~120 kDa) forms of the protein are present (Fig. 2A, solid line). At a 4-fold higher concentration of the protein the proportion of the dimeric fraction (V_e/V_o of 1.60, ~114 kDa) increases relative to that of the monomer (V_e/V_o of 1.73, ~87 kDa). Besides the peak representing aggregated protein at the V_o of the column (8 mL), a larger oligomeric form elutes as a shoulder in front of the dimeric protein peaks (V_e/V_o of 1.44, ~180 kDa), which could represent a trimeric form of the protein (Fig. 2A, dotted line).

Possible dimerisation as a result of disulphide-bond formation was subsequently analysed with the addition of 10 mM DTT to the protein (3-5 mg/mL) prior to SEC, which resulted in a significant shift from a dimer (V_e/V_o of 1.61, ~131 kDa) to the monomeric form (V_e/V_o of 1.68, ~99 kDa) (Fig. 2B, solid line). Non-reducing SDS-PAGE confirmed the shift of the dimer to the monomer in the presence of DTT (Fig. 2C). However, both the SDS-PAGE and SEC results show a slight increase in the apparent molecular weight of the reduced protein compared to the non-reduced monomeric protein, which was also confirmed by DLS (see below). The increased propensity of PfAdoMetDC to dimerise under non-reducing conditions suggests the involvement of Cys residue/s on the protein surface in disulphide bond/s formation between the PfAdoMetDC monomers.

3.3 Involvement of Cys505 in disulphide-linked dimerisation of PfAdoMetDC

Inspection of the proposed dimer interface of the PfAdoMetDC homology model [11], suggests that Cys505 from each monomer could form a disulphide bond. Therefore, the MALDI-MS peptide mass fingerprints of the dimeric PfAdoMetDC protein (Fig. 2C) without reduction prior to alkylation were compared to the fingerprints of the dimeric protein that was reduced and alkylated after purification of the gel bands from SDS-PAGE. The results confirmed that the

carbamidomethyl-modified Cys505 residue is only present in the monomeric band when alkylation was conducted under reducing conditions (results not shown).

While the expression level (Fig. 3A) and specific activity of PfAdoMetDC-C505S was unchanged compared to the wild-type PfAdoMetDC (results not shown), the addition of DTT once again resulted in a larger apparent size of the protein as shown by SDS-PAGE (Fig. 3A) compared to the non-reduced samples (Fig. 3B) of both the wild-type and mutated monomeric proteins. Subsequent SEC of the mutant protein at a concentration of 1 mg/mL and under non-reducing conditions showed that the PfAdoMetDC-C505S protein occurs mainly as a monomer (V_e/V_o of 1.74) (Fig. 3C, solid line). However, the equilibrium was again shifted towards dimer formation at a concentration of 4 mg/mL (V_e/V_o of 1.64, Fig. 3C, dotted line). These results indicate that the PfAdoMetDC protein is still able to dimerise even in the absence of covalently-linked dimers.

DLS showed a radius of 5.79 nm for the C505S mutant in the absence of DTT (3 mg/mL), while treatment of PfAdoMetDC at a concentration of 2.8 mg/mL with DTT only decreased the hydrodynamic radius from 9.07 to 7.33 nm. These results suggest that disulphide linkage either induces changes in protein conformation, which is not readily reversed by DTT treatment alone or reflects the average radius of a mixture of the monomeric and dimeric forms of the protein or an increase in its apparent size due to DTT treatment [29]. The increase in size of the C505S mutant in the presence of DTT (Fig. 3A, lane 2) suggests the latter as a likely explanation although the likelihood that reduction of inner disulphide bonds by DTT that could affect a shape change from e.g. globular to a more expanded and thus a larger size protein [30], cannot be excluded.

3.4 Estimated dissociation constants of PfAdoMetDC

The extent of dimer formation as a function of time of the PfAdoMetDC and C505S mutant proteins were estimated based on the SEC results in Fig. 2A and Fig. 3C. Table 1 lists the relative proportions of the monomeric and dimeric proteins in the 1 mg/mL samples used in analytical SEC for both PfAdoMetDC and the C505S mutant. Simple monomer-dimer equilibrium was assumed

where in the absence of DTT, residues Cys505 could form covalently-linked dimers in a slow, irreversible manner such that the true K_D of PfAdoMetDC would be slightly elevated in the presence of DTT.

The K_D values were in the micromolar range, suggesting a relatively weak affinity for dimer formation, with a higher tendency of PfAdoMetDC to dimerise than the C505S mutant (K_D value 87% less than that of the mutant) (Table 1). The K_D value of dimeric PfAdoMetDC (9.75 μM) in the absence of DTT is also 300-fold higher than the estimated K_D for the human protein (33 nM) [23], showing a comparatively reduced predisposition of the plasmodial protein to dimerise. However, this K_D value for PfAdoMetDC is similar to that of monomeric plant AdoMetDC (15.38 μM), its nearest conserved orthologue, which has been structurally characterised [14].

3.5 Far-UV CD analyses of PfAdoMetDC

Far-UV CD was performed to determine the secondary structure of the PfAdoMetDC protein for comparison to dimeric human AdoMetDC [23] as well as to observe any major secondary structural changes that might take place in the predominantly monomeric C505S mutant protein. At the concentration of 0.5 mg/mL used in these analyses, and by applying the estimated K_D value for the C505S mutant protein (Table 1), the dimeric proportion within this sample was estimated to be 15%. The spectra showed that PfAdoMetDC conforms to proteins with significant β-sheet content (40%), with a minimum at 209.5 nm and a maximum at 191 nm (Fig. 4). This correlates well with what has been predicted in the homology model of PfAdoMetDC [11] and dimeric human AdoMetDC, which showed a minimum at 218 nm and a maximum at 195 nm [23]. It is conceivable that parasite-specific inserts of unknown structure (constituting 32% of the 572-residue PfAdoMetDC protein [11]), contribute to the differences in the spectra with 34% of the PfAdoMetDC secondary structure indicated to be disordered with far-UV CD (Fig. 4).

The spectra of PfAdoMetDC and the C505S mutant proteins are similar, which provided confidence in the fact that, while the C505S mutation in PfAdoMetDC showed a reduced tendency

of the protein to dimerise, neither the mutation nor the monomeric status affected the secondary structure of PfAdoMetDC.

3.6 Enzyme kinetics of monofunctional PfAdoMetDC

Enzyme kinetics of the SEC-purified PfAdoMetDC was studied and compared with those of other AdoMetDCs. By using the K_D value of PfAdoMetDC it could be calculated that, at the concentration used in the enzyme kinetics experiments, >99% of the PfAdoMetDC protein would exist as monomers. A typical Michaelis-Menten curve was obtained (Fig. 5A) with the subsequent Hanes-Woolf plot indicating a K_m of 250 µM and a V_{max} of 77 nmol/min/mg (Fig. 5B). The K_m here is approximately 4-fold higher than reported for the wtPfAdoMetDC-hinge enzyme and 6-fold higher than the PfAdoMetDC enzyme in association with PfODC in the bifunctional complex expressed from the native gene (Table 2) [9]. Thus, it appears that the presence of the hinge region (and/or PfODC) in some way improves the substrate affinity of PfAdoMetDC within the bifunctional complex. However, the K_m determined here for monofunctional PfAdoMetDC is in a similar range to that of the homodimeric trypanosomal AdoMetDC orthologues (Table 2). The k_{cat} of monofunctional PfAdoMetDC was calculated to be 5.3 min^{-1}; the enzyme therefore converts a molecule of substrate into product every 11 s compared to the 0.4 s it takes for human AdoMetDC (Table 2). The k_{cat} values of the wtPfAdoMetDC-hinge and the bifunctional protein preparation of PfAdoMetDC (both expressed from the wild-type, unharmonised genes) are similar and in the range of 3.3 to 4 min^{-1} (Table 2).

Analysis of enzyme kinetics in the presence of the irreversible inhibitor MDL73811 [26] showed that PfAdoMetDC activity decreased in a concentration dependent manner (Fig. 6A). A secondary plot yielded a linear graph from which a k_{inact} value of 0.46 min^{-1} and a K_i of 0.33 µM were determined for MDL73811 (Fig. 6B). Comparison to the reported K_i of 1.6 µM for MDL73811 on PfAdoMetDC/ODC [7] indicates stronger inhibition of the monofunctional protein (Table 2). Kinetic analysis of the inhibition of PfAdoMetDC with CGP48664 [28] revealed non-competitive

inhibition with a K_i of 4.07±0.14 μM (Fig. 6D), which is similar to the reported value for wtPfAdoMetDC-hinge (Table 2) [7]. The inhibition of *T. cruzi* AdoMetDC by CGP48664 was also shown to be non-competitive [31] but inhibition of human AdoMetDC with CGP48664 is competitive [32].

4. Discussion

The crystal structure of human AdoMetDC revealed a four-layer αββα-sandwich domain [16], which at the time of publishing, had not been observed in any other protein structure in the Protein Data Bank. The quaternary structure of the active protein is an $(\alpha\beta)_2$ dimer, where the active sites are located at the autocatalytic cleavage site, distant from the dimer interface. Processing also results in the formation of the α- and β-subunits. An unusual collection of charged residues between the β-sheets of each monomer, well-removed from the active site, has been shown as the site for cooperative putrescine binding [23, 33-35]. The crystal structure of plant (*S. tuberosum*) AdoMetDC showed that the protein adopts the same α/β-fold as the human protein but it revealed two major differences, namely: 1) plant AdoMetDC is constitutively active as putrescine does not stimulate autocatalytic processing nor catalytic activity; and 2) it exists as a monomer [14]. Like the plant protein, the activity of AdoMetDC from *P. falciparum* is not stimulated by putrescine nor is it required for the autocatalytic processing event [9]. Homology modeling of the monofunctional PfAdoMetDC monomer, using the plant and human AdoMetDC structures as templates, showed the same α/β-fold and like the plant enzyme the autocatalytic processing was predicted to be dependent on the Lys15, Lys215, Arg11 triad, which simulates putrescine binding [11]. Furthermore, the active site and charged buried site residues were conserved, with similar conformation to that of the human counterpart. However, the lack of biochemical and biophysical studies on monofunctional PfAdoMetDC has prevented the elucidation of its functional oligomeric unit and the regulation of PfAdoMetDC activity either in its monofunctional form or in association with PfODC in the bifunctional protein is unclear.

The limited information on the structure as well as several biochemical characteristics of PfAdoMetDC is mainly due to the inferior heterologous expression of soluble PfAdoMetDC/ODC [36, 37]. In this study, we show that codon harmonisation dramatically improved the expression and stability of the monofunctional PfAdoMetDC domain of the bifunctional PfAdoMetDC/ODC and thus represented a valid strategy to obtain a high yield of pure protein for subsequent biochemical studies. The levels of Hsp70, which normally co-purify with PfAdoMetDC, were considerably reduced suggesting less stress on *E. coli* during protein translation and folding. Additionally, the Strep-tag was moved to the C-terminus to pre-empt possible interference of the tag at the N-terminus of PfAdoMetDC with protein activity due to its close proximity to the pyruvoyl cofactor. Codon harmonisation has also been shown to result in improved protein yield and solubility of three malaria vaccine candidates, namely MSP_{142} (FVO), MSP_{142} (3D7) and MSP_{142} (Camp) [17].

The monomer-dimer equilibrium of PfAdoMetDC was shown to be concentration-dependent and was shifted towards the dimeric form at higher protein concentrations and towards the monomeric form under reducing conditions. Iodoacetamide treatment and subsequent MS suggested that the solvent-exposed Cys505 on the β15 strand is involved in disulphide bond formation at the proposed edge-on dimer interface between two monomeric PfAdoMetDC proteins [11], which is similar to the established interaction site of monomers of the human protein. However, formation of the disulphide bond mediated by Cys505 is not proposed to be essential for PfAdoMetDC quaternary structure formation or activity due to the cytosolic location of PfAdoMetDC/ODC *in vivo* and the presence of glutathione and thioredoxin redox systems [38] but possibly maintains the protein in a fixed conformation *in vitro*. Mutation of Cys505 to Ser reduced the *in vitro* tendency of PfAdoMetDC to dimerise, with a K_D 300-fold higher than that of the dimeric human protein [23]. The K_D of the PfAdoMetDC dimeric protein (9.75 μM) is 7-fold lower than the C505S mutant but similar to that of the monomeric plant protein (15.38 μM) [14], which indicates that PfAdoMetDC has a lower dimer affinity than human AdoMetDC. The results also suggest that the (αβ) monomeric form, which dominates at the concentration used to determine the activity of

PfAdoMetDC (0.004 mg/mL), is active. It was previously suggested that both putrescine binding and dimerisation of human AdoMetDC are prerequisites for positive cooperativity between the monomers [23]. Since PfAdoMetDC does not require putrescine binding for activity, these results support a fully active monomeric form for this protein.

The C505S PfAdoMetDC mutant also formed dimers at moderately high protein concentrations presumably at the predicted dimer interface [11]. However, PfAdoMetDC normally occurs as the bifunctional partner protein of PfODC implying hydrophobic interactions between the two proteins. Therefore, dimerisation could additionally occur through side-to-side hydrophobic interactions between two monofunctional PfAdoMetDCs on one face of the protein as predicted by the homology model and extensive protein-protein docking studies. The latter dimers would be indistinguishable from those that involve the predicted dimer interface (Fig. 7) [11, 39]. It has furthermore been shown that interdomain interactions occur between PfAdoMetDC and PfODC in the bifunctional complex and are mediated by parasite-specific inserts [10]. Inserts are species-specific, non-homologous regions that diverge rapidly and may contain low-complexity segments with prevalence for positively-charged residues [40]. Furthermore, these inserts may form non-globular, flexible loops that protrude on the surface of the protein [10]. Since the relative positions of these parasite-specific inserts in the quaternary structure of PfAdoMetDC are unknown [11], their potential role in dimerisation (or oligomerisation) cannot be excluded (Fig. 7). We show here that since the C505S mutant has a significantly lower affinity for dimer formation than the wild type protein, PfAdoMetDC can dimerise at the same site which usually mediates dimerisation of the human protein but that it is not necessary for activity.

The recombinant monofunctional PfAdoMetDC protein produced here from a harmonised gene is therefore believed to be similar in conformation to the native protein. This is based on the secondary structure comparison as determined with far-UV CD that showed similarities between the *P. falciparum* and human AdoMetDCs as well as the confirmation that disulphide formation at the proposed dimer interface is mediated between closely situated Cys505 residues, which confirms the

dimer interface predictions of Wells *et al*. [11]. The presence of the processed form of the recombinant protein, which is reliant on the exact positioning of the Lys15, Lys215, Arg11 triad, also indicates the correct conformation of the recombinant protein.

Initial activity analyses of monofunctional *Pf*AdoMetDC reinforced previous suggestions that both the hinge region and PfODC play important roles in modulation of PfAdoMetDC activity [10]. Removal of PfODC as well as half of the hinge region increases wtPfAdoMetDC-hinge activity by 20% and decreases the K_m from 58 to 43 μM [9]. We show here that the further deletion of 88 residues from the hinge region resulted in a 55% increase in activity relative to the activity of PfAdoMetDC within the bifunctional PfAdoMetDC/ODC and a 6-fold increase in K_m [9]. The K_m value of PfAdoMetDC is surprisingly similar to that of homodimeric *T. brucei* and *T. cruzi* AdoMetDC suggesting that monofunctional PfAdoMetDC behaves like other parasitic enzymes in the absence of the hinge or PfODC. However, PfAdoMetDC is a less catalytically efficient enzyme compared to other AdoMetDCs that are activated by putrescine (human, *T. cruzi*) or an allosteric prozyme effector (*T. cruzi*, *T. brucei*). In the presence of prozyme, the k_{cat} of *T. brucei* AdoMetDC is increased 1,200-fold compared to that of the homodimer [41] while a similar situation was seen for *T. cruzi* where both prozyme and putrescine increased the enzyme efficiency to a level similar to that of the fully activated counterpart in *T. brucei* [42]. In the absence of putrescine or prozyme stimulation of PfAdoMetDC activity, it can be postulated that the bifunctional association of PfAdoMetDC and PfODC could allow the parasite to mediate regulatory mechanisms between the two decarboxylase domains but an allosteric effector remains to be identified that could increase the enzyme efficiency of PfAdoMetDC to the levels observed for human and heterodimeric trypanosomal AdoMetDCs. Understanding the *in vitro* conformation and oligomeric status of PfAdoMetDC could therefore allow for the identification of such an allosteric effector since covalent fixation of the protein with disulphide bonds may impede possible conformational communication between the active sites of the bifunctional complex.

Our results indicate that PfAdoMetDC in the bifunctional PfAdoMetDC/ODC has a 6-fold lower K_m and a slightly lower enzyme efficiency (k_{cat} of 5.3 min^{-1} versus 3.3 min^{-1}) compared to the monofunctional PfAdoMetDC [9]. The higher K_m of monofunctional PfAdoMetDC therefore prevents binding of metabolically important AdoMet when putrescine-producing PfODC is absent. Within the bifunctional complex, the affinities of both enzymes for their respective substrates improve (43 µM for PfAdoMetDC and 42 µM for PfODC) with synchronised enzyme catalytic rates of approximately 3 min^{-1} [9] producing dcAdoMet and putrescine every 18-20 s for the subsequent synthesis of spermidine by spermidine synthase. These property changes of the two enzymes in the bifunctional complex is hypothesised to be due to subtle changes in the active site centre induced by long-range effects [43] modulated by interdomain protein interactions with PfODC [10] to regulate the polyamine levels within the parasite.

The unique properties of PfAdoMetDC in a bifunctional complex with PfODC and the presence of parasite-specific inserts suggest that AdoMetDC from *Plasmodium* does not fall within the current subclasses of AdoMetDC [12, 13]. AdoMetDC proteins are classified into two main groups; those from bacterial or archeal origin are in group 1 while the eukaryotic AdoMetDCs fall into group 2. Group 1 is subdivided based on oligomeric status and the requirement of a metal ion for activity (Subclass 1a: gram-negative bacteria, tetramer) or an unknown activation factor (Subclass 1b: gram-positive bacteria and archaea, dimer). Group 2 constitutes the eukaryotic enzymes that are not affected by putrescine (Subclass 2a: plant, monomer) and those that do bind putrescine are further subdivided into the human (Subclass 2b-I, dimer) and the trypanosomatids (Subclass 2b-II, heterodimer with prozyme) AdoMetDC classes [12]. Based on these different groupings, and with respect to monofunctional activity and oligomeric arrangement, PfAdoMetDC seems to belong to the parasitic AdoMetDC subclass 2b-II. However, due to the unique bifunctional arrangement and the lack of activation by putrescine or prozyme, we propose a distinct subclass for plasmodial AdoMetDCs, namely subclass 2b-III.

Acknowledgements

We thank Jaco de Ridder for the design of the codon-harmonised gene as well as Evelina Angov for advice on the harmonisation of the gene. This work was supported by the South African Malaria Initiative (http://www.sami.org.za), the South African National Research Foundation (Grant FA2007050300003), National Research Foundation-Swedish International Cooperation Development Agency (NRF-SIDA, Swedish Research Links Program) and the University of Pretoria. Any opinion, findings and conclusions or recommendations expressed in this paper are those of the author(s) and therefore the NRF does not accept any liability in regard hereto.

References

[1] Wallace HM, Fraser AV, Hughes A. A perspective of polyamine metabolism. Biochem J 2003;376:1-14.

[2] Igarashi K, Kashiwagi K. Modulation of cellular function by polyamines. Int J Biochem Cell Biol;42:39-51.

[3] Heby O. Role of polyamines in the control of cell proliferation and differentiation. Differentiation 1981;19:1-20.

[4] Poulin R, Pelletier G, Pegg AE. Induction of apoptosis by excessive polyamine accumulation in ornithine decarboxylase-overproducing L1210 cells. Biochem J 1995;311:723-7.

[5] Xie X, Tome ME, and Gerner EW. Loss of intracellular putrescine pool-size regulation induces apoptosis. Exp Cell Res 1997;230:386-92.

[6] Assaraf YG, Golenser J, Spira DT, Bachrach U. Polyamine levels and the activity of their biosynthetic enzymes in human erythrocytes infected with the malarial parasite, *Plasmodium falciparum*. Biochem J 1984;222:815-9.

[7] Das Gupta R, Krause-Ihle T, Bergmann B, Müller IB, Khomutov A, Müller S, et al. 3-Aminooxy-1-aminopropane and derivatives have an antiproliferative effect on cultured *Plasmodium falciparum* by decreasing intracellular polyamine concentrations. Antimicrob Agents Chemother 2005;49:2857-64.

[8] Müller S, Da'dara A, Lüersen K, Wrenger C, Das Gupta R, Madhubala R, et al. In the human malaria parasite *Plasmodium falciparum*, polyamines are synthesised by a bifunctional ornithine decarboxylase, *S*-adenosylmethionine decarboxylase. J Biol Chem 2000;275:8097-102.

[9] Wrenger C, Lüersen K, Krause T, Müller S, Walter RD. The *Plasmodium falciparum* bifunctional ornithine decarboxylase, *S*-adenosylmethionine decaroxylase enables a well-balanced polyamine synthesis without domain-domain interaction J Biol Chem 2001;276:29651-6.

[10] Birkholtz L, Wrenger C, Joubert F, Wells GA, Walter RD, Louw AI. Parasite-specific inserts in the bifunctional *S*-adenosylmethionine decarboxylase/ornithine decarboxylase of *Plasmodium falciparum* modulate catalytic activities and domain interactions. Biochem J 2004;377:439-48.

[11] Wells GA, Birkholtz L, Joubert F, Walter RD, Louw AI. Novel properties of malarial *S*-adenosylmethionine decarboxylase as revealed by structural modelling. J Mol Graph Model 2006;24:307-18.

[12] Bale S, Ealick S. Structural biology of *S*-adenosylmethionine decarboxylase. Amino Acids 2009;38:451-60.

[13] Pegg AE. *S*-adenosylmethionine decarboxylase. Essays Biochem 2009;46:25-46.

[14] Bennett EM, Ekstrom JL, Pegg AE, Ealick SE. Monomeric *S*-adenosylmethionine decarboxylase from plants provides an alternative to putrescine stimulation. Biochemistry 2002;41:14509-17.

[15] Bale S, Baba K, McCloskey DE, Pegg AE, Ealick SE. Complexes of *Thermotoga maritima S*-adenosylmethionine decarboxylase provide insights into substrate specificity. Acta Crystallogr Sect D Biol Crystallogr 2010;66:181-9.

[16] Ekstrom JL, Mathews II, Stanley BA, Pegg AE, Ealick SE. The crystal structure of human *S*-adenosylmethionine decarboxylase at 2.25 Å resolution reveals a novel fold. Structure 1999;5:583-95.

[17] Angov E, Hillier CJ, Kincaid RL, Lyon JA. Heterologous protein expression is enhanced by harmonising the codon usage frequencies of the target gene with those of the expression host. PLoS ONE 2008;3:e2189.

[18] Nirmalan N, Sims PFG, Hyde JE. Quantitative proteomics of the human malaria parasite *Plasmodium falciparum* and its application to studies of development and inhibition. Mol Microbiol 2004;52:1187-99.

[19] Everberg H, Peterson R, Rak S, Tjerneld F, Emanuelsson C. Aqueous two-phase partitioning for proteomic monitoring of cell surface biomarkers in human peripheral blood mononuclear cells. J Proteome Res 2006;5:1168-75.

[20] Luoto S, Lambert W, Blomqvist A, Emanuelsson C. The identification of allergen proteins in sugar beet (Beta vulgaris) pollen causing occupational allergy in greenhouses. Clinical and Molecular Allergy 2008;6:7.
[21] Williams M, Louw AI, Birkholtz L. Deletion mutagenesis of large areas in *Plasmodium falciparum* genes: a comparative study. Malaria J 2007;6:64.
[22] Greenfield NJ. Using circular dichroism spectra to estimate protein secondary structure. Nature Protocols 2006;1:2876-90.
[23] Bale S, Lopez MM, Makhatadze GI, Fang Q, Pegg AE, Ealick SE. Structural basis for putrescine activation of human *S*-adenosylmethionine decarboxylase. Biochemistry 2008;47:13404-17.
[24] Lees JG, Smith BR, Wien F, Miles AJ, Wallace BA. CDtool - An integrated software package for circular dichroism spectroscopic data processing, analysis and archiving. Anal Biochem 2004;332:285-9.
[25] Wilson K, Walker J. Practical Biochemistry: Principles and Techniques. 5th ed: Cambridge; 2000.
[26] Danzin C, Marchal P, Casara P. Irreversible inhibition of rat *S*-adenosylmethionine decarboxylase by 5'-([(Z)-4-amino-2-butenyl]methylamino)-5'-deoxyadenosine. Biochem Pharmacol 1990;40:1499-503.
[27] Kitz R, Wilson IB. Esters of methanesulfonic acid as irreversible inhibitors of acetylcholinesterase. J Biol Chem 1962;237:3245-9.
[28] Regenass U, Mett H, Stanek J, Mueller M, Kramer D, Porter CW. CGP48664, a new *S*-adenosylmethionine decarboxylase inhibitor with broad spectrum antiproliferative and antitumor activity. Cancer Res 1994;54:3210-7.
[29] Li X, Han Y, Pan XM. Cysteine-25 of adenylate kinase reacts with dithiothreitol to form an adduct upon aging of the enzyme. FEBS Lett 2001;507:169-73.
[30] van Beers MMC, Sauerborn M, Gilli F, Brinks V, Schellekens H, Jiskoot W. Aggregated recombinant human interferon beta induces antibodies but no memory in immune-tolerant transgenic mice. Pharmacol Res 2010;27:1812-24.
[31] Clyne Beswick T, Willert EK, Phillips MA. Mechanisms of allosteric regulation of *Trypanosoma cruzi S*-adenosylmethionine decarboxylase. Biochemistry 2006;45:7797-807.
[32] Tolbert WD, Ekstrom JL, Mathews, II, Secrist JA, Kapoor P, Pegg AE, et al. The structural basis for substrate specificity and inhibition of human *S*-adenosylmethionine decarboxylase. Biochemistry 2001;40:9484-94.
[33] Xiong H, Pegg AE. Mechanistic studies of the processing of human *S*-adenosylmethionine decarboxylase proenzyme. J Biol Chem 1999;274:35059-66.
[34] Tolbert WD, Cottet SE, Bennet EM, Ekstrom JL, Pegg AE, Ealick SE. Mechanism of human *S*-adenosylmethionine decarboxylase proenzyme processing as revealed by the structure of the S68A mutant. Biochemistry 2003;42:2386-95.
[35] Xiong H, Stanley BA, Tekwani BL, Pegg AE. Processing of mammalian and plant *S*-adenosylmethionine decarboxylase proenzymes. J Biol Chem 2009;272:28342-8.
[36] Vedadi M, Lew J, Artz J, Amani M, Zhao Y, Dong A, et al. Genome-scale protein expression and structural biology of *Plasmodium falciparum* and related Apicomplexan organisms. Mol Biochem Parasitol 2006;151:100-10.
[37] Gardner MJ, Hall N, Fung E, White O, Berriman M, Hyman RW, et al. Genome sequence of the human malaria parasite *Plasmodium falciparum*. Nature 2002;419:498-511.
[38] Müller S. Redox and antioxidant systems of the malaria parasite *Plasmodium falciparum*. Mol Microbiol 2004;53:1291-305.
[39] Wells GA. Molecular modeling elucidates parasite-specific features of polyamine pathway enzymes of *Plasmodium falciparum*: University of Pretoria; 2010.
[40] Pizzi E, Frontali C. Low-complexity regions in *Plasmodium falciparum* proteins. Genome Res 2001;11:218-29.

[41] Willert EK, Fitzpatrick R, Phillips MA. Allosteric regulation of an essential trypanosome polyamine biosynthetic enzyme by a catalytically dead homolog. Proc Natl Acad Sci USA 2007;104:8275-80.
[42] Willert EK, Phillips MA. Cross-species activation of trypanosome S-adenosylmethionine decarboxylase by the regulatory subunit prozyme. Mol Biochem Parasitol 2009;168:1-6.
[43] Jackson LK, Baldwin J, Akella R, Goldsmith EJ, Phillips MA. Multiple active site conformations revealed by distant site mutation in ornithine decarboxylase. Biochemistry 2004;43:12990-9.
[44] Brun R, Bühhler Y, Sandmeier U, Kaminsky R, Bacchi CJ, Rattendi D, et al. *In vitro* trypanocidal activities of new *S*-adenosylmethionine decarboxylase inhibitors. Antimicrob Agents Chemother 1996;40:1442-7.

Table 1
Dissociation constants of PfAdoMetDC and the C505S mutant from analytical non-reducing SEC at 1 mg/mL concentrations. The concentrations of monomer [M] and dimer [D] were calculated as follows: [M] = [C] x X_M, [D] = (M_0 - [M])/2 = ([C] x X_D)/2. Where M_0 is the total molar concentration, X_M and X_D are the relative proportions of monomer and dimer, and C (µM) is the protein concentration applied to the SEC column. Assuming simple monomer-dimer equilibrium (in the absence of a reducing agent) the apparent association (K_A) and dissociation constants (K_D) of dimeric PfAdoMetDC could then be calculated as follows: K_A = [D]/([M][M]) = 1/K_D.

Sample	C (µM)	X_D	X_M	[D] (µM)	[M] (µM)	K_D (µM)	Ref.
PfAdoMetDC	14.65	0.53	0.42	3.88	6.15	9.75	-
PfAdoMetDC-C505S	14.65	0.22	0.74	1.61	10.84	72.98	-
H. sapiens AdoMetDC			-			0.033	[23]
S. tuberosum AdoMetDC			-			15.38	[14]

Table 2

Comparison of enzyme kinetics for AdoMetDC from different organisms.

Organism	Protein arrangement, oligomeric state	K_m[a] -put	K_m[a] +put	k_{cat} (min^{-1})	MDL73811[b]	CGP48664[b]	Putrescine effect	Ref.
H. sapiens	Homodimer	74	59	114 (-put) 156 (+put)	0.56	5000 (-put) 0.005 (+put)	Stimulates	[26, 28, 31]
P. falciparum	Monofunctional PfAdoMetDC, monomer	250	-	5.3	0.33	4.1	-	Current study
	Monofunctional PfAdoMetDC-hinge	58	-	4	-	3	-	[7, 9]
	Bifunctional PfAdoMetDC/ODC, heterotetramer	43	-	3.3	1.6	-	-	[7, 9]
T. cruzi	Homodimer	260	250	-	-	100 (-put) 6 (+put)	Stimulates	[31]
	Homodimer	540	130	0.3 (-put) 1.44 (+put)	-	-	Stimulates	[42]
	Monomer/prozyme, heterodimer	580	170	36 (-put) 50.4 (+put)	-	-	Stimulates	[42]
T. brucei	Homodimer	380	240	0.096 (-put) 0.492 (+put)	-	0.49	Stimulates	[42, 44]
	Monomer/prozyme, heterodimer	110	170	84 (-put) 102 (+put)	-	-	-	[42]

[a] The K_m values (in µM) are given in the presence and absence of putrescine (put) in the organisms where putrescine stimulates the activity of AdoMetDC.

[b] The K_i values (in µM) are given in the presence and absence of putrescine (put) in the organisms where putrescine stimulates the activity of AdoMetDC.

Fig. 1. (A) SDS-PAGE analyses of expressed monofunctional wtPfAdoMetDC-hinge and PfAdoMetDC proteins and (B) Western blotting with an anti-Strep-tag antibody. The sizes of the protein ladder are indicated in lane MW. Lane 1: wtPfAdoMetDC-hinge protein expressed from the wild-type, unharmonised gene; band a: Hsp70; band b: α-subunit of PfAdoMetDC-hinge. Lane 2: PfAdoMetDC protein expressed from the harmonised gene; band a: Hsp70; band b: unprocessed PfAdoMetDC; band c: α-subunit of PfAdoMetDC.

Fig. 2. Analyses of the oligomeric status of PfAdoMetDC under reducing and non-reducing conditions. (A) The PfAdoMetDC protein purified with Strep-*Tactin* affinity chromatography at a concentration of 1 and 4 mg/mL was separated with SEC. (B) SEC was performed in the presence or absence of 10 mM DTT, followed by visualisation of the 4 mg/mL protein sample with non-reducing SDS-PAGE in which 10 mM DTT was either omitted or added to the sample buffer (C). The V_e/V_o values are shown on the X-axis while the Y-axes on the left and right of the graphs show the absorbance at 280 nm for the higher and lower concentrated protein samples, respectively. The sizes of the protein ladder as well as the positions of the dimeric and monomeric proteins on the SDS-PAGE gel are indicated.

Fig. 3. Analyses of the oligomeric status of a C505S mutant of PfAdoMetDC. (A) Reducing and (B) non-reducing SDS-PAGE of the PfAdoMetDC (lane 1) and C505S mutant (lane 2) proteins. The sizes of the protein ladder are shown. (C) Analyses of the oligomeric status of the PfAdoMetDC-C505S mutant protein purified with Strep-*Tactin* affinity chromatography and at concentrations of 1 and 4 mg/mL with SEC. The V_e/V_o values are shown on the X-axis while the Y-axes on the left and right of the graphs show the absorbance at 280 nm for the higher and lower concentrated protein samples, respectively.

Fig. 4. Far-UV CD analyses of the monofunctional PfAdoMetDC and C505S mutant proteins in a phosphate buffer between wavelengths of 190 nm and 150 nm.

Fig. 5. Michaelis-Menten kinetics of monofunctional PfAdoMetDC. (A) The substrate affinity constant as well as V_{max} of PfAdoMetDC was determined using Michaelis-Menten kinetics. A substrate dilution series ([S]) ranging from 12.5 to 800 µM was used to determine the mean of the reaction velocities (v, nmol/mg/min) from three independent experiments carried out in duplicate. S.E.M is indicated. (B) The linear Hanes-Woolf plot was subsequently used to determine the K_m and V_{max} values.

Fig. 6. Inhibition kinetics of PfAdoMetDC treated with MDL73811 and CGP48664. (A) For the irreversible inhibitor MDL73811 the Kitz-Wilson method was used where the percentage enzyme activity (given by the maximal protein activity following pre-incubation with a specific inhibitor concentration ([I]) for time interval t (E_t) over the protein activity following pre-incubation in the absence of inhibitor for each [I] tested (E_0)) against time is shown. Linearisation was performed by plotting the inverse of the slope from the primary plot versus the inverse of [I]. (B) For CGP48664 the Michaelis-Menten curves showing the reaction velocities (v, nmol/mg/min) in the presence of a substrate ([S]) dilution series ranging from 100 to 800 µM and an inhibitor dilution series ranging from 2.5 to 10 µM are indicated. The linear Dixon plots (D) were obtained by plotting the inverse of the reaction velocities against [I].

Fig. 7. The homology model of monofunctional PfAdoMetDC showing the predicted dimer interface and PfODC interaction sites. The α- and β-subunits of the monomeric PfAdoMetDC protein are shown in light grey and black, respectively. The molecular surfaces of the PfAdoMetDC residues that are predicted to interact with PfODC resulting in a "side-to-side" interaction and involving one face of PfAdoMetDC are shown in grey. The PfAdoMetDC model was superimposed with the dimeric human AdoMetDC structure (1JEN, shaded light grey and black for the α- and β-

subunits, respectively) to show the predicted dimer interface involving the β-strands between the two monomers, which results in an "edge-on" association of the monomeric proteins. The active site pyruvoyl cofactors are shown as grey spheres while the predicted positions of the parasite-specific inserts (Inserts 2 and 3 shown as grey dashed curves) and the N- and C-termini are indicated.

Figure 1

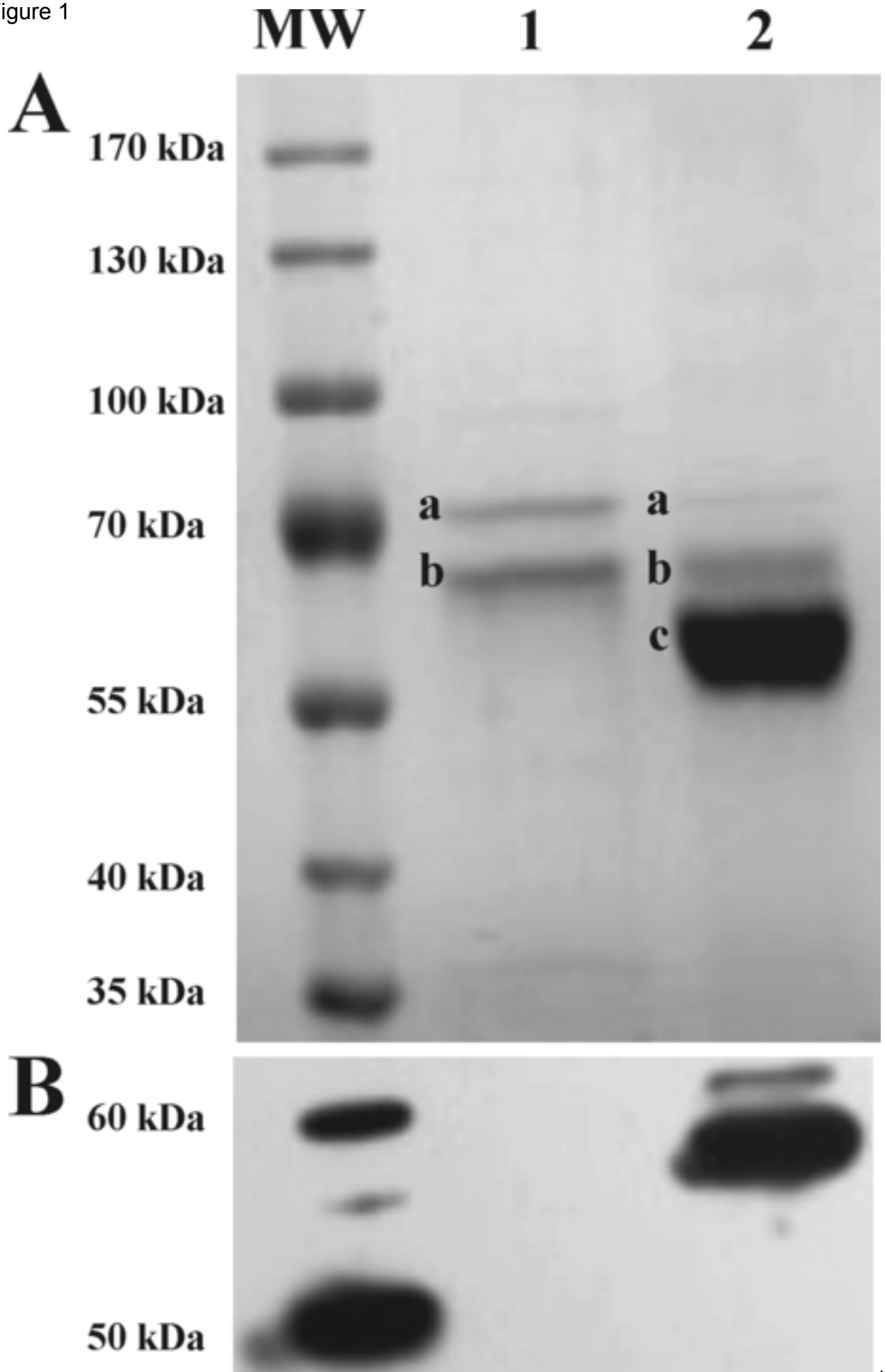
MW
1
2
A
170 kDa
130 kDa
100 kDa
70 kDa
55 kDa
40 kDa
35 kDa
a
b
a
b
c
B
60 kDa
50 kDa

Figure 2

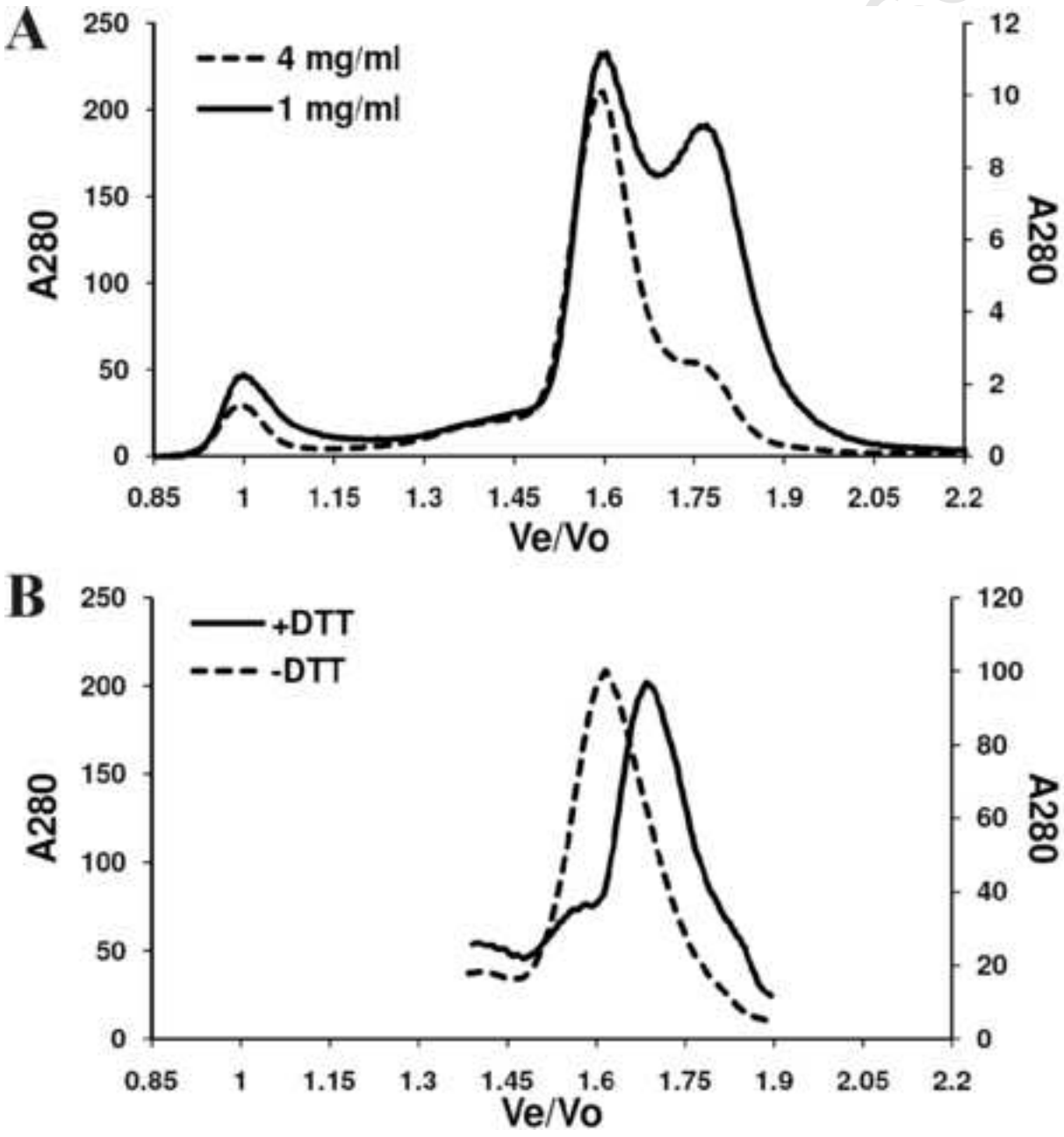
A
4 mg/ml
1 mg/ml
A280
Ve/Vo
B
+DTT
-DTT
A280
Ve/Vo
C
-DTT
+DTT
200 kDa
150 kDa
120 kDa
100 kDa
70 kDa
60 kDa
Dimer
Monomer

Figure 3

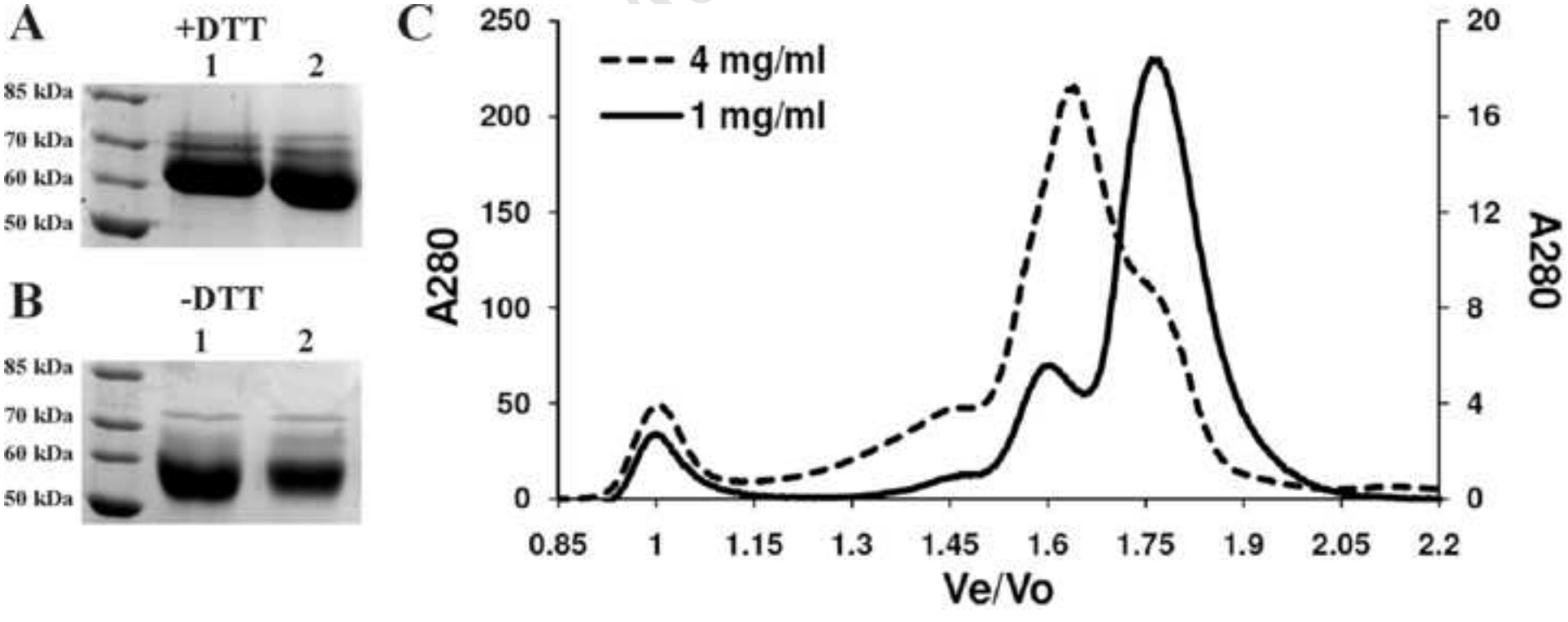
A
+DTT
1
2
85 kDa
70 kDa
60 kDa
50 kDa
B
-DTT
1
2
85 kDa
70 kDa
60 kDa
50 kDa
C
4 mg/ml
1 mg/ml
A280
250
200
150
100
50
0
20
16
12
8
4
0
A280
0.85
1
1.15
1.3
1.45
1.6
1.75
1.9
2.05
2.2
Ve/Vo

Figure 4

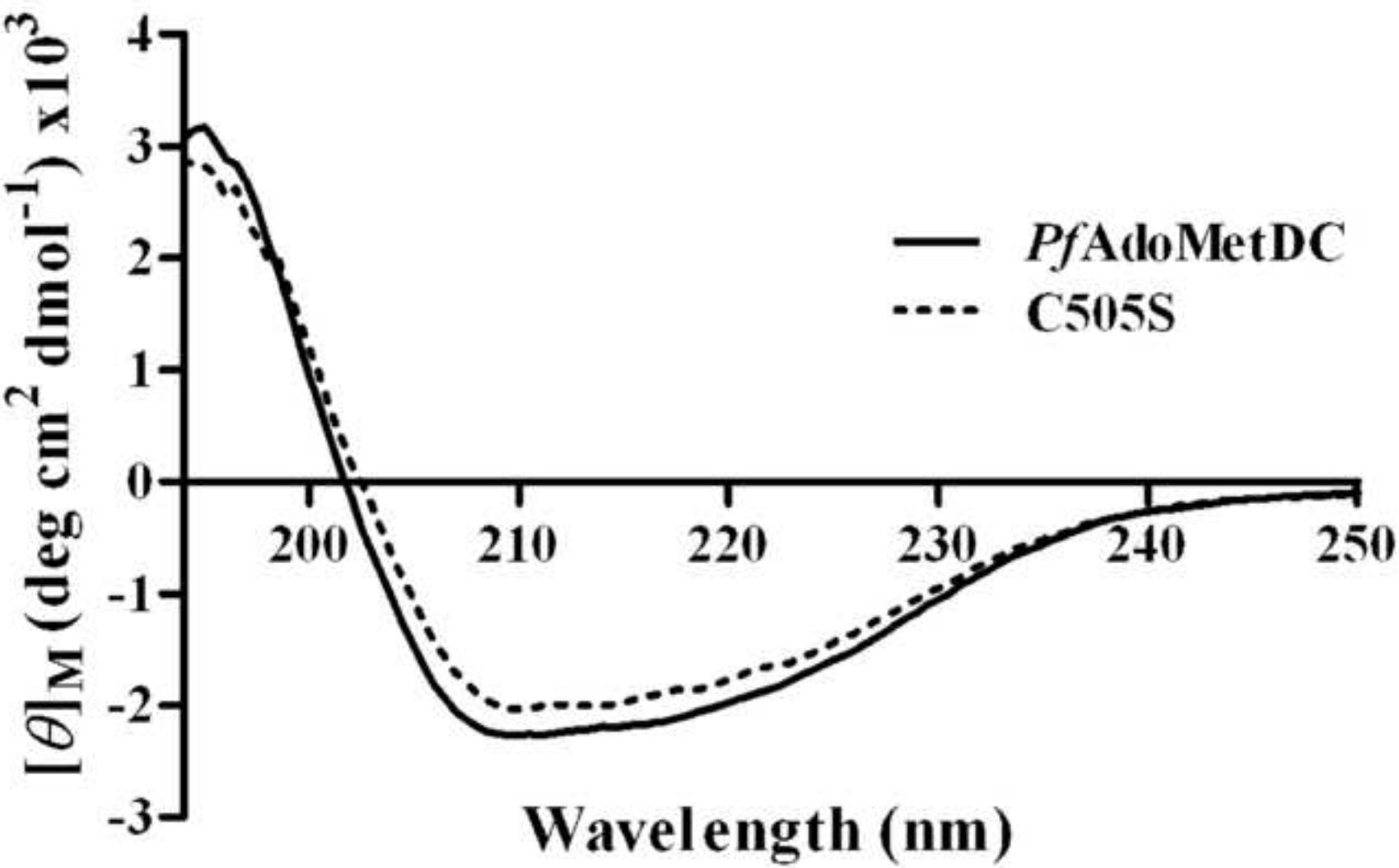
$[\theta]_M$ (deg cm^2 dmol^{-1}) x10^3
4
3
2
1
0
-1
-2
-3
200
210
220
230
240
250
Wavelength (nm)
*Pf*AdoMetDC
C505S

Figure 5

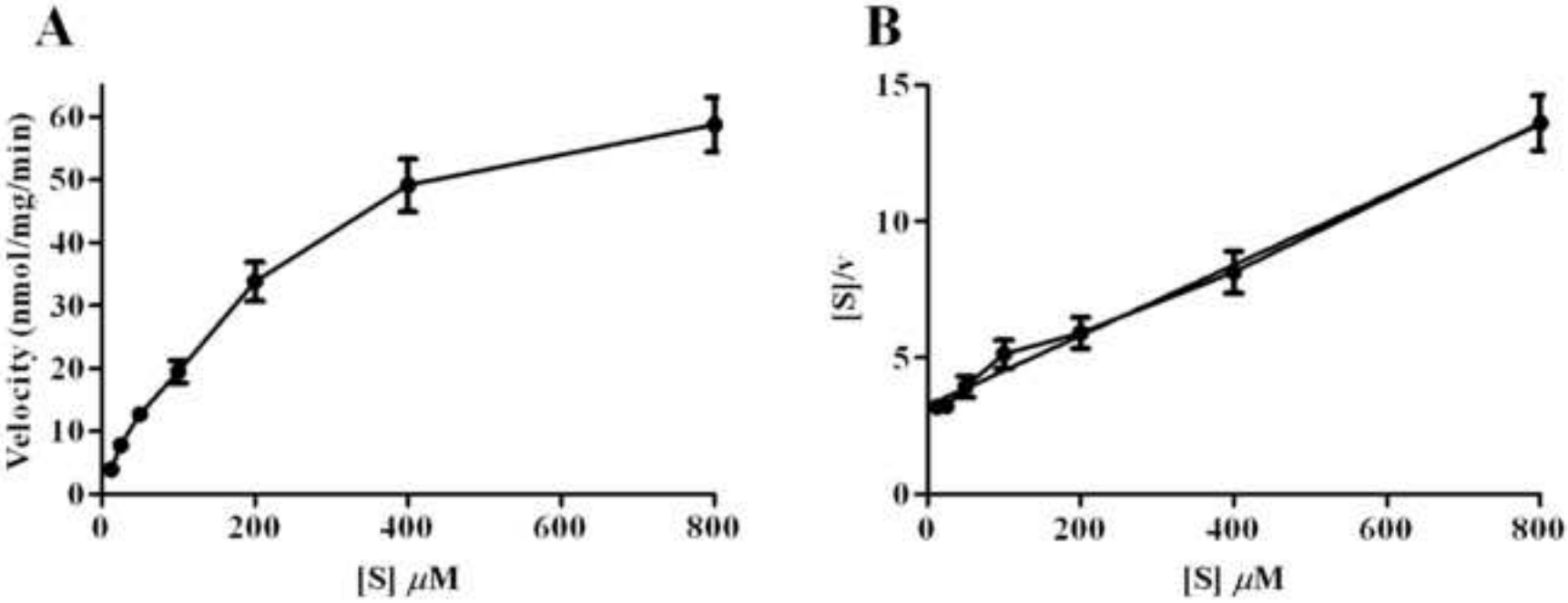
A
Velocity (nmol/mg/min)
0
10
20
30
40
50
60
0
200
400
600
800
[S] μM
B
[S]/v
0
5
10
15
0
200
400
600
800
[S] μM

Figure 6

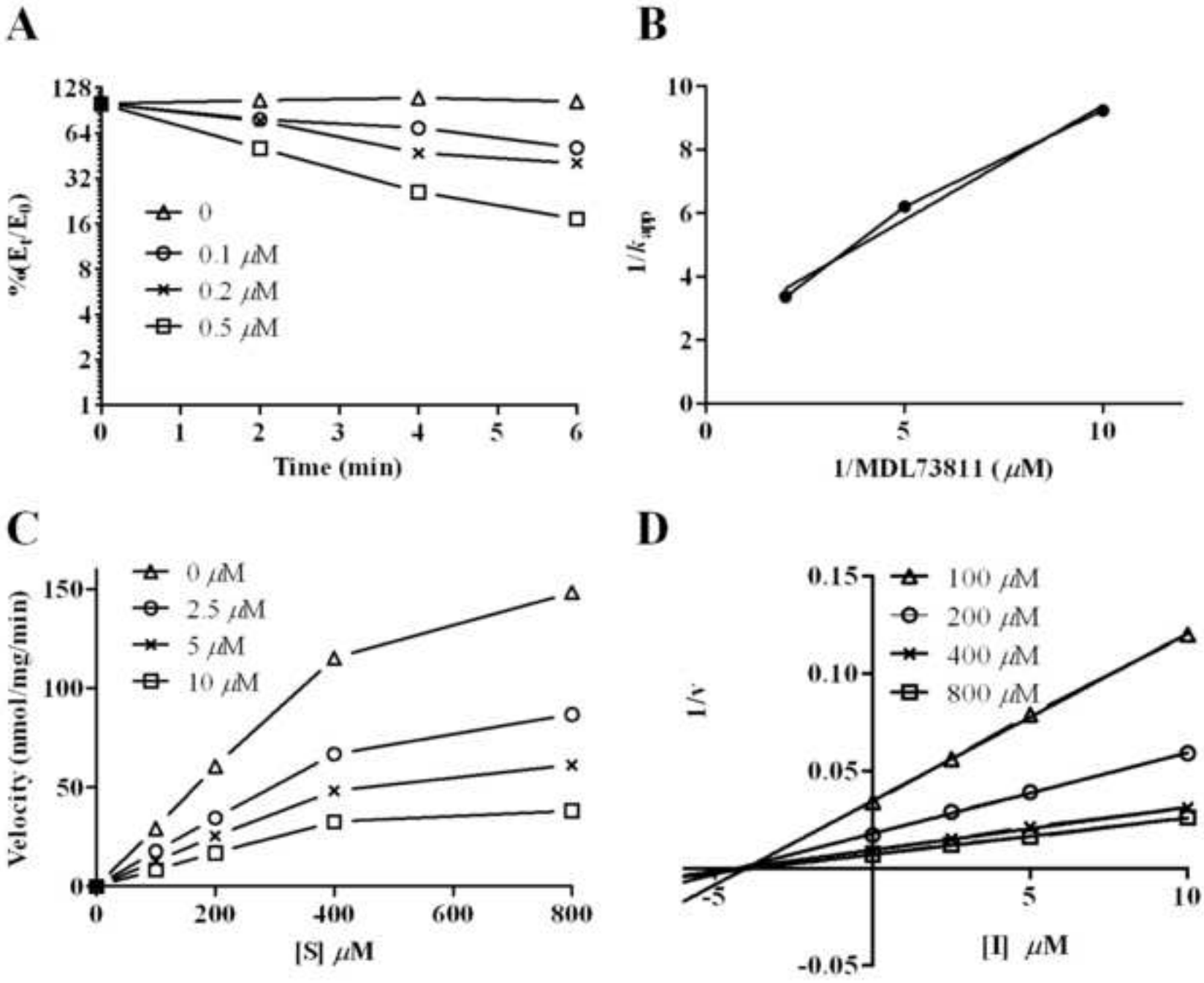
A
128
64
32
16
8
4
2
1
%(E_t/E_0)
0
0.1 μM
0.2 μM
0.5 μM
0
1
2
3
4
5
6
Time (min)
B
10
8
6
4
2
0
1/k_app
0
5
10
1/MDL73811 (μM)
C
150
100
50
0
Velocity (nmol/mg/min)
0 μM
2.5 μM
5 μM
10 μM
0
200
400
600
800
[S] μM
D
0.15
0.10
0.05
-0.05
1/v
100 μM
200 μM
400 μM
800 μM
-5
5
10
[I] μM

Figure 7